Controls on earthflow formation in the Teanaway River basin, central Washington State, USA

Sarah A. Schanz[1], A. Peyton Colee[1]

[1]Geology Department, Colorado College, Colorado Springs, 80903, USA

Correspondence to: Sarah A. Schanz (sschanz@coloradocollege.edu)

Abstract. Earthflows create landscape heterogeneity, increase local erosion rates, and heighten sediment loads in streams. These slow moving and fine-grained mass movements make up much of the Holocene erosion in the Teanaway River basin, central Cascade Range, Washington State, yet controls on earthflow activity and the resulting topographic impacts are unquantified. We mapped earthflows based on morphologic characteristics and relatively dated earthflow activity using a flow directional surface roughness metric called MADstd. The relative MADstd activity is supported by six radiocarbon ages, three lake sedimentation ages, and 16 cross-cutting relationships, indicating that MADstd is a useful tool to identify and relatively date earthflow activity, especially in heavily vegetated regions. Nearly all of the mapped earthflows are in the Teanaway and lower Roslyn formations, which compose just 32.7% of the study area. Earthflow aspect follows bedding planes in these units, demonstrating a strong lithologic control on earthflow location. Based on absolute ages and MADstd distributions, a quarter of the earthflows in the Teanaway Basin were active in the last few hundred years; the timing coincides with deforestation and increased land use in the Teanaway. Major tributaries initiate in earthflows and valley width is altered by earthflows that create wide valleys upstream and narrow constrictions within the earthflow zone. Although direct sediment delivery from earthflows brings fine sediment to the channel, stream power is sufficient to readily transport fines downstream. Based on our findings, over the Holocene—and particularly in the last few hundred years—lithologic-controlled earthflow erosion in the Teanway basin has altered valley bottom connectivity and increased delivery of fine sediments to tributary channels.

1 Introduction

Mass movement, including earthflows, transports debris from hillslopes to valley bottoms and can be crucial in creating and maintaining landscape heterogeneity, riparian refuge habitat, and spawning gravels for salmon (Beeson et al., 2018; May et al., 2013). Large wood (LW) transported by mass wasting into the channel results in channel roughness and the formation of resting pools and habitat complexity (Burnett et al., 2007). Deep-seated landslides are associated with wider valleys, a key landscape component for salmon and trout habitat (Beeson et al., 2018; Burnett et al., 2007; May et al., 2013). However, fine debris by landslides can present a habitat challenge as silt clogs the pores between stream cobbles and limits oxygen flow to redds (NFTWA, 1996), and landslides in narrow tributaries may dam the stream and temporarily kill off a small population

(Waples et al., 2008). In landslide-dominated landscapes, understanding the history of landsliding is crucial to reconstructing the development of valley bottom topography and maintenance of habitat.

In particular, earthflows can have a long-lasting effect on topography, sediment supply, and habitat. Earthflows are fine-grained soil mass movements that move meters or less per year and persist for decades to centuries (Hungr et al., 2014). They tend to occur in clay-bearing rocks or weathered volcanic rocks with translational movement, and are commonly reactivated in response to increased precipitation or other disturbances that decrease shear resistance (Baum et al., 2003). Earthflow movement is correlated to climate and regolith production; over long timescales (10^1-10^4 years), earthflow movement is limited by the pace of regolith production as transport typically outpaces weathering rates (Mackey and Roering, 2011). At the annual to decadal scale, precipitation variability is correlated with earthflow speed, in which earthflows are observed to speed up—following a lag of several weeks—after seasonal and annual precipitation increases (Coe, 2012; Handwerger et al., 2013). Droughts may prime earthflows by creating deep desiccation cracks that act as water conduits during ensuing wet conditions (McSaveney and Griffiths, 1987). Similar to deep seated landslides, earthflows can cause upstream channel aggradation and valley widening; Nereson and Finnegan (2018) note an order of magnitude increase in valley width upstream of the Oak Ridge, California, earthflow.

Due to their persistence, earthflows can be major sources of sediment to channels, and therefore a significant disturbance to habitat and landscape evolution. Earthflows in the Eel River basin, although covering only 6% of the basin, account for half of the regional denudation rate with approximately 19,000 t/km/yr of sediment produced (Mackey and Roering, 2011). In stream sediment production is unsteady as annual to decadal precipitation conditions and sediment supply cause intermittent movement over the decades to centuries that the earthflow is active (Guerriero et al., 2017; Mackey and Roering, 2011). Additionally, earthflows can temporarily transition to debris flows, resulting in rapid transport of weathered material and debris to the channel (Malet et al., 2005). Lithologic controls on earthflow location in the Eel River results in isolated resistant sandstone outcrops and topographic highs, indicating earthflows can influence valley-scale topographic patterns (Mackey and Roering, 2011).

Here, we examine the cause and timing of Holocene earthflows in the Teanaway Basin of the central Cascade Range of Washington State, located in the northwest corner of the continental USA. Geologic mapping of the region and recent lidar reveals extensive landsliding in the form of earthflows (Quantum Spatial, 2018, 2015; Tabor et al., 1982), but the cause and timing of these earthflows is unknown. We develop a relative dating curve for earthflows and apply it to the Teanaway basin to determine when the earthflows were active and discuss how this affected valley width, sediment supply, and habitat during the Holocene.

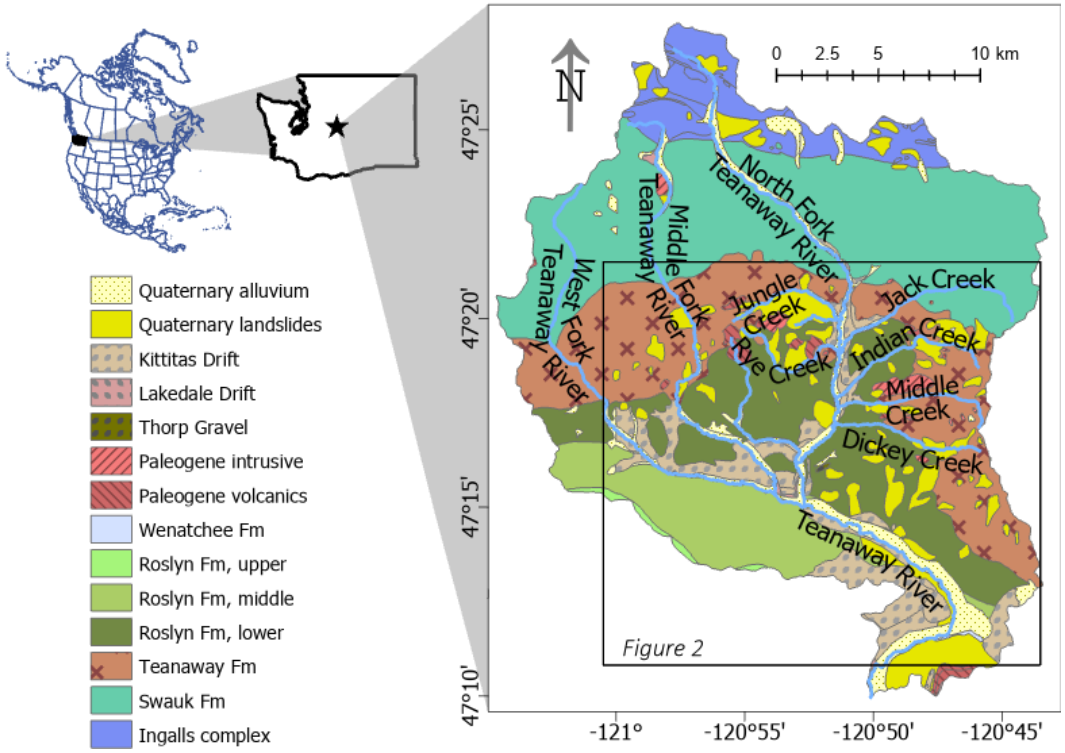

Figure 1. Geologic map of the Teanaway watershed (Tabor et al., 1982). Upper left inset shows location of Washington State in North America, and the location of the study area (star) within Washington State. Box shows location of Figure 2.

2 Study Site

The Teanaway River is located in central Washington State, northwest USA, four miles east of Cle Elum, WA (Figure 1). This single-thread river has three main tributaries known as the West Fork, the Middle Fork, and the North Fork which all flow into the main Teanaway River about 10 miles upstream of its confluence with the Yakima River. The region receives between 980 and 1230 mm of precipitation annually and is typically snow-covered during the winter (U.S. Geological Survey, 2012) with large fires occurring every 300-350 years (Agee, 1996; 1994), though high-intensity burns are limited to less than 1 km^2 (Wright and Agee, 2004). Mapped faults do not offset Quaternary alluvium and exhumation and Holocene denudation rates are low at 0.05 mm/yr and 0.08-0.17 mm/yr respectively (Moon et al., 2011; Reiners et al., 2003). The branches of the Teanaway River were splash dammed from 1892-1916 (Cle Elum Tribune, 1891; Kittitas County Centennial Committee, 1989) and the *Pinus ponderosa* forests were logged from the 1890s through the 1940s.

The majority of rock units in the study area were deposited during the Eocene (Figure 1). The lower Eocene Swauk Formation, composed of dark sandstone with small amounts of siltstone and conglomerate, unconformably overlies the Jurassic Ingalls Complex and is ~4800 m thick (Tabor et al., 1984). The Swauk Formation is folded with dip directions generally to the south

(Tabor et al., 1982). The middle Eocene Teanaway Formation unconformably lies on the steeply tilted Swauk Formation. The Teanaway Formation ranges from 10 to 2500 m thick and is composed of basaltic and andesitic lava flows interbedded with tuff, breccia, and feldspathic sedimentary rocks (Tabor et al., 1984). Because of its resistance to weathering, this formation forms most of the taller and more rugged peaks in the Teanaway area. Rhyolite flows from this formation have interbedded with the conformable upper Eocene Roslyn Formation and outcrop through the study area as dikes (Tabor et al., 1984). The youngest surficial rock unit, the Roslyn Formation, covers most of the lower-elevation study area. The unweathered white and weathered yellow immature sandstones were deposited conformably on the Teanaway Formation in the late Eocene (Tabor et al., 1984). The Roslyn and Teanaway formations lie relatively flat or gently tilted to the southwest compared to the Swauk Formation, and are very susceptible to erosion and sliding due to the interbedded tuffs, paleosols, clays, and silts (NFTWA, 1996; Tabor et al., 1982).

Overlying the Eocene units are glacial and mass wasting deposits. Glacial terraces originate from the Thorp and Kittitas glaciations at 600 ky and 120 ky, respectively (Porter, 1976). During drift deposition, glaciers from the Cle Elum catchment to the west overtopped the dividing ridge and entered the West Fork and lower Middle and North Fork Teanaway valleys. Thorp and Kittitas moraines, composed of poorly sorted gravels and cobbles, are present at the eastern edge of the study area near the outlet of the mainstem Teanaway into the Yakima River and on the ridges surrounding the West Fork Teanaway (Porter, 1976). The Thorp drift sediments are heavily eroded and therefore less visible than the Kittitas drift sediment, which has been modified by mass wasting (Porter, 1976).

Geologic mapping has identified several Quaternary mass wasting deposits in the Roslyn and Teanaway formations (Figure 1) and subsequent reports have focused on landslides near stream banks (NFTWA, 1996). Landslides are as old as late Pliocene and are concentrated near rhyolite tuffs and a weathered surface in the Teanaway Formation, which form planes of weakness (NFTWA, 1996). Although closed depressions and ponds are visible in the lidar and suggest some recent activity, landslides are not easily distinguished in aerial photography or in the field. Lidar in 2015 and 2018 (Quantum Spatial, 2018, 2015) revealed the extent of these slides, but no studies since have quantified landslide volumes or constrained the timing or mechanism of sliding.

3 Methods

Our analysis focuses on the entirety of the Teanaway basin, though the majority of the earthflows are found within tributaries to the North Fork Teanaway River. To identify the temporal and spatial distribution of earthflows, we use geomorphic mapping in conjunction with a directional roughness metric to identify and relatively date earthflow activity in the Teanaway basin. Other studies (e.g., Mackey and Roering, 2011) use tree and object tracking to measure earthflow velocity; we attempted to do this but found the dense vegetation and high tree growth rates prevented us from accurately matching objects between

image pairs. Thus, we rely on surface roughness to give relative earthflow activity. We constrain the relative ages using radiocarbon and sedimentation ages, which both give maximum estimates of earthflow activity.

3.1 Earthflow mapping and maximum earthflow ages

We first created a detailed earthflow map for the study region. All visually-identifiable landslides within the Teanaway basin were mapped in ArcGIS from one-meter resolution lidar (Quantum Spatial, 2018, 2015) at a scale of 1:5000. Earthflows were classified from this dataset based on: hourglass shape, narrow width and long length of slide zone, visible levees or shear zones at the edges, and flow-like morphologies (Baum et al., 2003; Nereson and Finnegan, 2018). These morphologic clues degrade over time and bias our earthflow mapping to younger slides; however, we focus our analysis on Holocene earthflow activity to minimize this bias.

We dated select earthflows using buried charcoal found within the earthflow toe deposits. Long residence times of buried charcoal in landslides can result in radiocarbon ages >8000 years older than landslide activity (Struble et al., 2020); considering that earthflows can also have episodic activity which further complicates the relationship between timing of earthflow activity and radiocarbon age, we use our charcoal ages to loosely constrain maximum earthflow activity. Sampled earthflows were selected based on a visual estimate of roughness and potential for a fresh exposure via road or stream erosion. In the field, we removed 10-50 cm of material from the toes of earthflows exposed by stream cuts or roadcuts to find 2-5 grams of charcoal. We collected radiocarbon samples from seven different earthflows (Table 1); one sample (8-4-20-2) did not yield enough carbon material to date. The samples were sent to the Center for Applied Isotope Studies (CAIS) lab at the University of Georgia and were dated using Accelerated Mass Spectrometry (AMS); dates were calibrated to calendar years using Intcal20 (Reimer et al., 2020).

In three cases where earthflows dammed the valley and formed lakes, we estimated the onset of valley blockage and an approximate earthflow age by using the sedimentation age of the lake. We reconstructed a pre-earthflow valley bottom using the techniques in Struble et al. (2020) and subtracted this from the lidar surface elevation to give an estimate of the sedimentation volume post-earthflow. We used nearby mid-Holocene denudation rates of 0.08 and 0.17 mm/yr based on basins in Moon et al. (2011) with similar mean annual precipitation and glaciation. The upper and lower denudation bounds were combined with the upstream contributing drainage area and sedimentation volumes to calculate the range of plausible sedimentation ages, which approximate when the earthflow dammed the creek. Earthflow activity may continue after lake formation; thus, these sedimentation ages do not necessarily represent the most recent earthflow activity.

3.2 Estimating earthflow activity using flow directional surface roughness

To relatively date earthflow activity, we created a surface roughness age calibration model similar to that used to date rotational slides in Washington State (LaHusen et al., 2016; Booth et al., 2017). Active earthflows have a unidirectional flow morphology

that gradually diffuses to less directional roughness as activity ceases, in contrast to rotational slides which start with uneven roughness in all directions. To account for the unique flow morphology of earthflows, we used a flow directional Median Absolute Differences (MAD) index (Trevisani and Rocca, 2015). MAD is a bivariate geostatistical index that analyzes Digital Elevation Models (DEMs) on multiple dimensions (Trevisani and Cavalli, 2016), giving us a directional roughness index for each raster cell across the study area. This directional roughness is combined with flow directions derived from the DEM to analyze surface roughness relative to flow direction (Trevisani and Cavalli, 2016) in which a high MAD value represents very directional regions, while a low MAD represents relatively uniform regions.

We first tested the relationship between MAD and earthflow age by extracting elevations from an earthflow along Jungle Creek where we obtained radiocarbon sample 8-1-20-1 (Figure 2, Table 1). We chose this earthflow because it has clear flow lines and blocks the majority of the stream valley with an outlet eroded through. This suggests the earthflow has been active recently to block the valley, yet is not so strongly active that the stream is permanently dammed. We applied two-dimensional diffusion to the earthflow surface, based on Eq (1):

$$\frac{dz}{dt} = -\mathrm{K}\frac{dz^2}{d^2x}, \quad (1)$$

where *dz* is change in elevation, *dt* is the timestep, and *dx* is the spatial resolution. The diffusion rate, *K*, is estimated as 0.002 m^2/yr based on regions in a similar climate (Martin, 2000), though we varied diffusion rate as low as 0.0002 m^2/yr for landscapes experiencing creep (Martin, 2000). We also ran the diffusion model with and without stream erosion. Stream erosion is represented by Eq (2):

$$\frac{dz}{dt} = K_{sp}A^m S^n , \quad (2)$$

where *A* is the upstream contributing drainage area, *S* is slope, and K_{sp}, *m*, and *n* are empirical coefficients related to drainage basin geometry, rock erodibility, channel hydraulics, and climate (Braun and Willett, 2013). The values of *m* and *n* are set at 0.5 and 1, respectively, based on common values for mountain streams (Braun and Willett, 2013), and K_{sp} is estimated at 6e-7 from empirical relationships of average denudation, *A*, and *S* along Jungle Creek. We ran the diffusion model for 10 ky and calculated MAD using the steps below every 2 ky.

MAD is calculated using the residual roughness; we first smoothed the one-meter DEM over a 3x3 window followed by a 5x5 window (Trevisani and Cavalli, 2016) and subtracted the smoothed DEM from the original DEM to obtain a residual raster of roughness elements. The MAD index (https://github.com/cageo/Trevisani-2015) was run with this residual raster and calculated the directional roughness over an 8 m radius window. We chose this window so that we examine a similar spatial scale as the 15x15 window used by LaHusen et al. (2016). We calculated flow direction across the smoothed DEM and created a raster with the MAD values in the direction of flow for each cell. Finally, we used Zonal Statistics to calculate the standard deviation of the directional roughness (MADstd) for each earthflow; from our diffusion model simulations, MADstd had the highest correlation with age (R^2 = 0.98).

3.3 Valley width

To examine the influence of landslides on habitat, we measured valley width along the tributaries of the North Fork Teanaway. The mainstem and three forks of the Teanaway all have wide valleys that are unaffected by earthflows. In contrast, the tributary valleys of the North Fork are altered by earthflows. We extracted valley width from Jungle, Rye, Dickey, Middle, Indian, Jack, and an unnamed creek (Figure 1) by defining the valley floor as being less than 5% slope. We used an automated process in ArcGIS to extract a valley centerline, create transects every 100 m, and measure valley width.

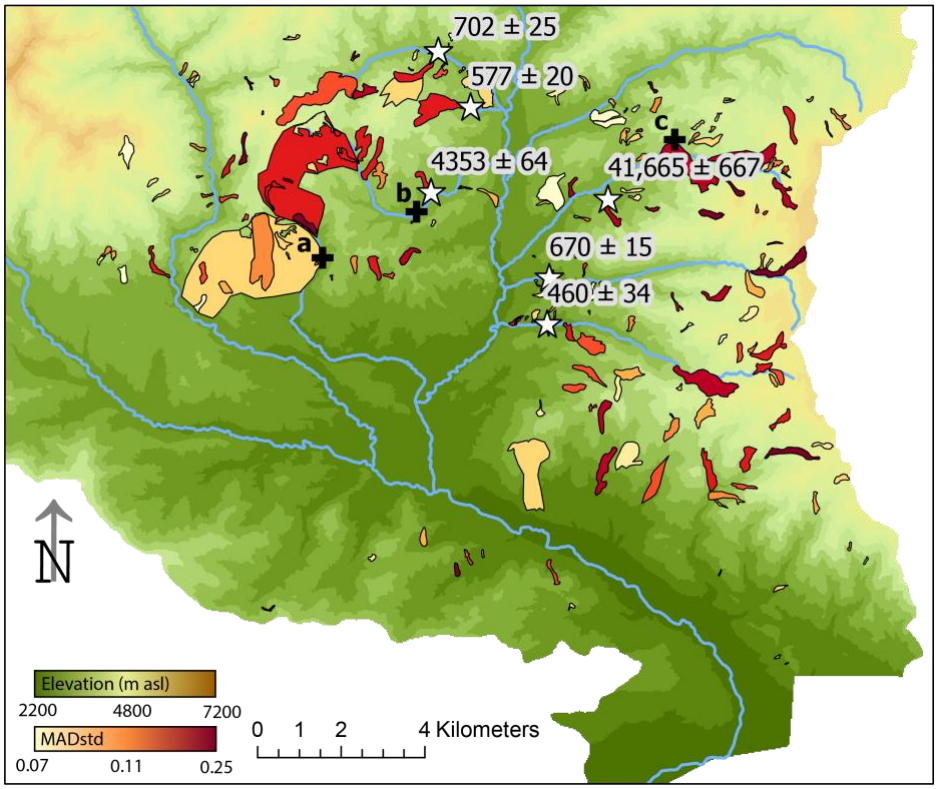

Figure 2. Earthflows mapped in the study area; earthflows are colored by their MADstd value. Radiocarbon locations and dates, in calibrated yr BP, are shown with white stars. Black crosses indicate locations of earthflow-dammed lakes where sedimentation ages are derived: a – unnamed creek; b – Rye Creek; and c – Indian Creek. Extent of region is shown in Figure 1. Background elevation data from Quantum Spatial (2015; 2018).

4 Results

4.1 Landslide mapping

We mapped 187 earthflows in the lower Teanaway basin (Figure 2). Mapped earthflows are mostly all north of the mainstem and Middle Fork of the Teanaway River, with the exception of eight small earthflows south of the Main Fork. The southern edge of the earthflow area appears to be bound by the extent of Pleistocene glaciation (Figure 1); perhaps glaciation removed

pre-existing earthflows or the muted topography from glacial erosion is less prone to mass movement. To the north, the earthflow domain is bound by the start of the Swauk Formation, which has little to no mappable landslides in it.

Earthflows spatially cluster in the Teanaway and lower Roslyn formation. Just over half (51%) of mapped earthflows are in the Teanaway Formation, which is composed of basalt and rhyolite interbedded flows and conformably grades upwards into the lower Roslyn Formation, in which 42% of earthflows are found. The remaining 7% are split between the Swauk and middle Roslyn Formations.

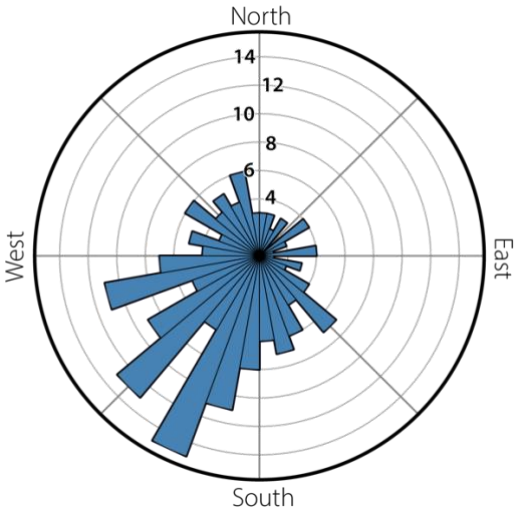

Figure 3. Average earthflow aspect, binned by 10 degrees. Contours indicate number of earthflows in each bin.

We extracted slope and aspect for each earthflow. The slope distribution, measured based on the smoothed one-meter lidar, was similar between earthflows and intact hillslopes of the Lower and Middle Roslyn Formations with modal slopes of 10 to 15 degrees. The average earthflow aspect shows strong preference for the southwest quadrant, with 45% of earthflows (Figure 3). The northwest and southeast quadrants were similarly populated with 20 and 21%, respectively, while the remaining earthflows are found in the northeast quadrant.

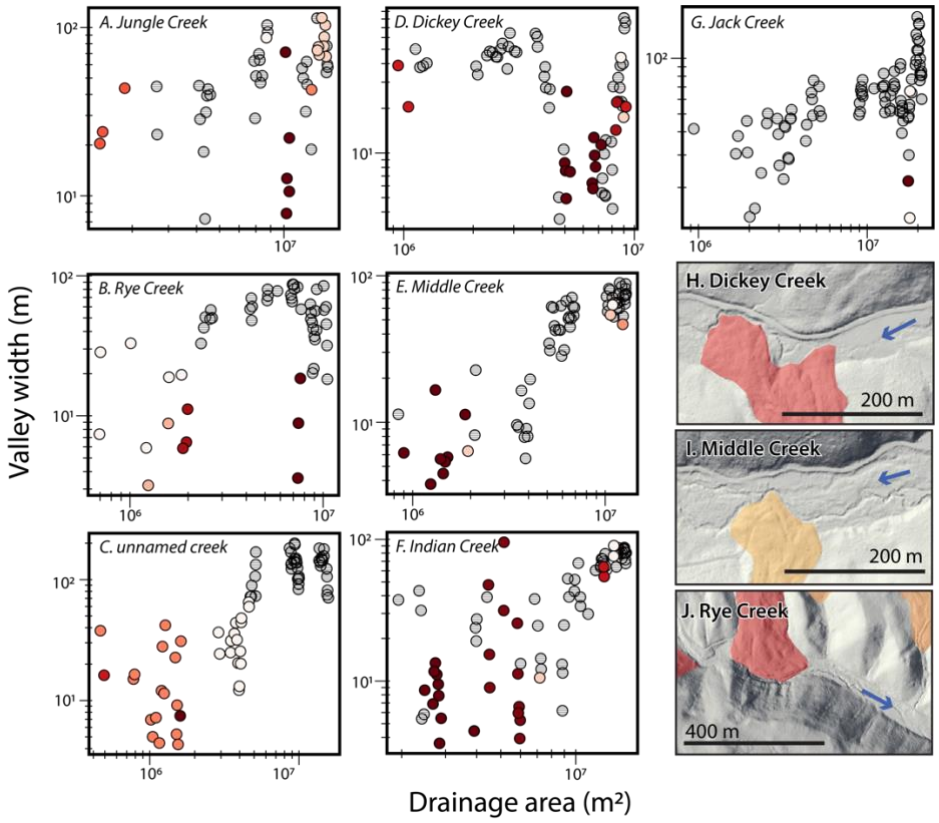

Figure 4. Valley width of the North Fork tributaries compared to upstream contributing drainage area (A-G). Tributaries are arranged counter clockwise from the northwest (see Figure 1 for locations). Colored circles indicate valley width measurements where one valley wall is an earthflow; colors indicate MADstd relative to earthflows within that tributary in which red are high MADstd and light pink are low MADstd. Panels H-J show examples of earthflows interacting with valley bottoms; earthflow color corresponds to MADstd value using same color scheme as panels A-G. Blue arrows show direction of water flow.

4.2 Valley width

Valley width generally increases with drainage area for the seven tributaries we examined, although the increase is not consistent (Figure 4). Jungle Creek has its narrowest width, equivalent to the channel width, halfway up the valley where a high MADstd earthflow pinches the valley. The valley width immediately upstream is 100 m wide, comparable to the widest part of the valley at the mouth of Jungle Creek. Similarly, Rye Creek's valley is pinched to the channel width at 2 km upstream (drainage area = 7.5e6 m^2) and widens immediately upstream to the widest values noted along the tributary. Similar trends of narrowed valleys with wider sections immediately upstream are seen in the other tributaries, though the trends are less strong. Rye, Middle, Indian, and the unnamed creek are confined by earthflows in the upper 1-2 km; these earthflows form the valley walls and bottom and constrain the valley width to the active channel width.

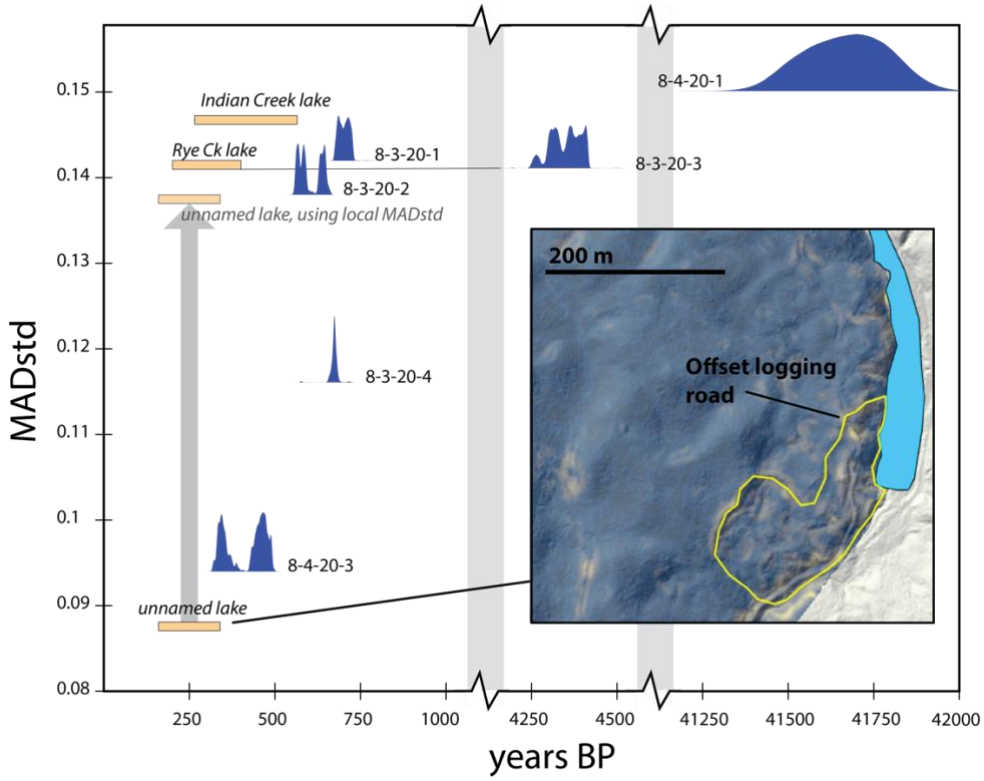

Figure 5. Comparison of maximum age estimates and MADstd values. Range of maximum earthflow ages from lake sedimentation are shown as orange bars and radiocarbon ages are shown with blue probability distribution functions. Inset shows the MADstd values calculated with a 5m moving window for the earthflow complex creating the unnamed lake. Note the relatively low MADstd in blue despite dense *Pinus ponderosa* forest covering earthflow surface. Yellow outline shows a possible re-activation of part of the complex, which raises the MADstd associated with lake formation from 0.087 to 0.137.

4.3 Maximum earthflow ages

Age results from radiocarbon dating range from 370 to 36,750 carbon-14 years before present, or 460 ± 34 to 41,665 ± 237 calibrated years before present (yr BP) (Table 1, Figure 5). Samples were taken from the toe of earthflows, and represent charcoal that was originally deposited in regolith then transported through earthflow movement. Thus, the age given by radiocarbon dating is a measure of 1) the inherited age of the charcoal, 2) regolith development, 3) earthflow transport, and 4) deposition at the earthflow toe. We cannot use our ages to directly date the last earthflow activity, but it does provide a maximum estimate of earthflow age.

Based on a range of denudation rates of 0.08 to 0.17 mm/yr, the lake formed along Indian Creek (Figure 2) took approximately 267 and 567 years to fill to the current level (Figure 5), indicating the earthflow has been constricting Indian Creek for at least that long. The lake along Rye Creek, formed just upstream of earthflow carbon site 8-3-20-3, took between 204 and 433 years to fill with sediment to the modern level, and the lake along the unnamed creek took approximately 159 to 337 years to fill.

The ages we derived from sedimentation rates and lake volume do not directly date earthflow activity, though the relationship is more complex than the radiocarbon ages. The lake itself formed when the earthflow initially dammed the valley, and so represents a maximum age. However, all lakes are currently filled with sediment and an outlet stream has eroded through the damming earthflow, which indicates the sedimentation age is a minimum estimate of the lake's age. Based on the observation that the outlet stream is still forming a knickpoint in the earthflow and has not yet incised through the lake fill, we believe the sedimentation age is close to the age of the lake and thus these ages more closely estimate the maximum earthflow age.

We were able to get a radiocarbon age and a sedimentation age for one earthflow: the Rye Creek earthflow was dated with charcoal to 4353 yr BP but has a sedimentation age of 204 to 433 years. These ages indicate upwards of 4000 years of residence time for charcoal in the earthflow, similar to values found for rotational landslides in the Oregon Coast Range (Struble et al., 2020), and a maximum estimate of earthflow activity to approximately 204 to 433 years ago. The other earthflows creating lakes are similarly young, with maximum ages in the last 500 years; radiocarbon ages support relatively recent earthflow activity with maximum age estimates of less than 1000 years for four of the six dated earthflows.

Table 1. Radiocarbon dates

Lab ID	Tributary name	Latitude	Longitude	C-14 yrs BP (2 sigma)	calibrated yr BP (2 sigma)	MAD std
8-3-20-1	Jungle Creek	47.34689	-120.87804	790 ± 20	702 ± 25	0.142
8-3-20-2	unnamed tributary to Jungle Creek	47.33463	-120.87036	640 ± 20	577 ± 20 (p = 0.57) 643 ± 18 (p = 0.43)	0.138
8-3-20-3	Rye Creek	47.31456	-120.87959	3910 ± 20	4353 ± 64	0.141
8-3-20-4	Middle Creek	47.29731	-120.84273	73 0 ± 20	670 ± 15	0.116
8-4-20-1	Indian Creek	47.31481	-120.82517	36750 ± 20	41665 ± 237	0.15
8-4-20-3	Dickey Creek	47.28752	-120.84302	370 ± 20	460 ± 34 (p = 0.61) 349 ± 29 (p = 0.39)	0.094

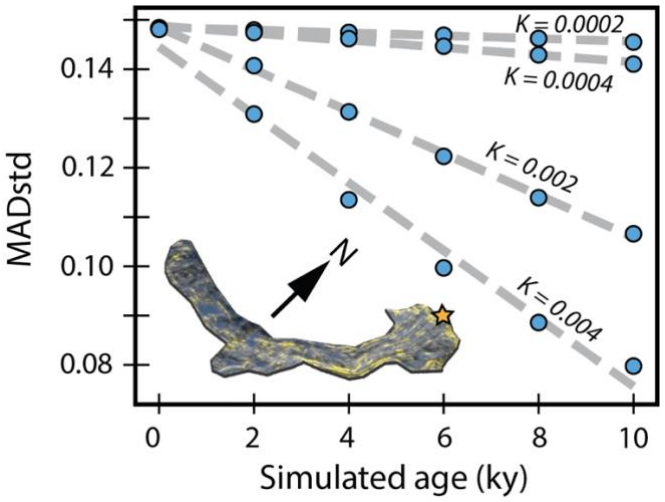

Figure 6. MADstd values for simulated diffusion across the Jungle Creek earthflow. Inset images shows the Jungle Creek slide with modern (simulation time = 0) MAD values where yellow are high directional MAD and blue are low. Star shows location of sample 8-3-20-1. For all diffusion values, linear regressions give an r-squared of >0.98.

4.4 Verification of MADstd relative dating

Simulated diffusion across the Jungle Creek earthflow shows a strong linear relationship between MADstd and earthflow age (Figure 6) with an r-squared fit of >0.98 for all four hillslope diffusion values tested. When simulations were run with stream erosion, resulting MADstd values were very similar with less than 5% difference in values and a median difference of 0.2%. Therefore, whether stream erosion is considered or not is negligible to the MADstd value. The linear decrease in MADstd values with time supports our initial theory that as earthflows stop moving, the directional roughness becomes more similar across the earthflow surface. Soil diffusion creates a more multi-directional surface with lower variation in flow directional roughness. When earthflows are active, orthogonal flow off the flow features and scarps creates a highly variable MAD and thus a high MADstd.

While our simulations give equations relating age and MADstd, we do not apply this equation to the study area because the relationship is highly dependent on the soil diffusion value. We do not know the site-specific diffusion rate, and even slight differences between K = 0.0002 and 0.0004 give widely different age estimates (Figure 6). We also do not know how the diffusion rate changed over the late Quaternary in our study area. However, we can assume that the diffusion rate and associated variations are similar across our study area, where climatic and biotic forcings are relatively uniform and earthflow source lithology is either lower Roslyn or Teanaway formation. Thus, we should be able to use MADstd to relatively date earthflow activity.

When we apply the MADstd value to mapped earthflows (Figure 2), topographic relationships support the relative dating technique (Figure 7). In our study area, there are 22 instances of earthflows clearly overlapping with another, in which

morphologic clues can be used to relatively date them. Of these, 16 had MADstd values consistent with the cross-cutting relationship. In cases where the MADstd gave incorrect relative ages, five were on earthflow complexes. MADstd appears to not work as well across large earthflow complexes where there is more heterogeneity in activity and less defined flow lines and scarps. If we disregard earthflow complexes, then only one of 17 cross-cutting relationships are not reflected by the relative MADstd values.

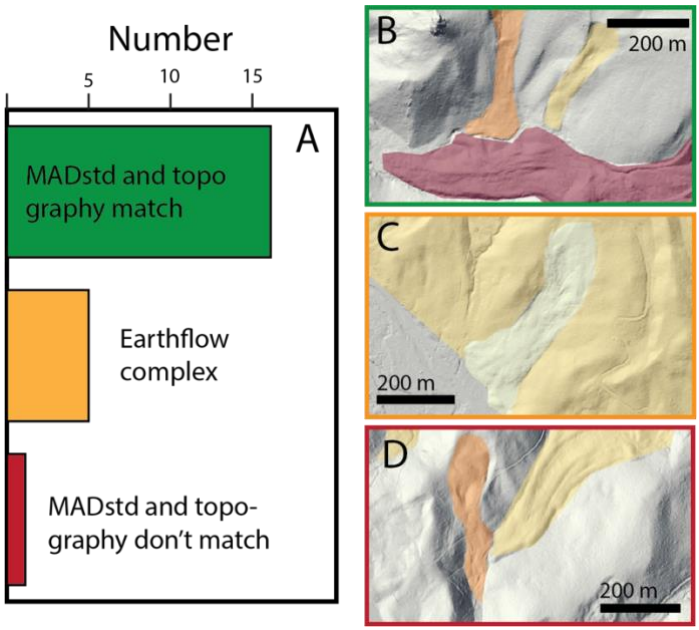

Figure 7. A) Cross cutting relationships compared to MADstd relative age relationships and B-D) examples of cross cutting relationships underlain by a lidar hillshade (Quantum Spatial, 2015; 2018).

Valley bottom impingement also supports the MADstd ages. Active earthflows are more likely to block tributary valleys in contrast to older, less active earthflows whose deposits can be eroded by the stream to re-form a wide valley. Earthflows that completely block valleys, or narrow valleys to the channel width, have higher MADstd values than earthflows that only partially block valleys (Figure 4H-J). One outlier to this is the 4-6 kilometers along Rye Creek and the unnamed creek (Figure 4B, C) with a low MADstd but strong effect on valley width. Both of these earthflows are large earthflow complexes (3-4 km^2) and the MADstd value of the entire complex may not represent the locally active portions that affect the two creeks.

Although MADstd appears to work to relatively date earthflows across the study area, comparing lake sedimentation ages and MADstd indicates that earthflows active at a similar time may display a range of MADstd values. Lakes along Rye and Indian Creek have sedimentation ages of 204 to 433 and 267 to 567 years, respectively, with MADstd values of associated valley-blocking earthflows of 0.141 and 0.146 (Figure 5). Given the error in sedimentation ages, we consider these lakes to have

formed at approximately the same time, thus indicating that MADstd values can range by at least 0.005 for earthflows with similar activity history.

The sedimentation age for the lake along the unnamed creek is an outlier, with the youngest range of sedimentation ages (159 to 337 years) yet the lowest MADstd of 0.087 which represents the least active earthflow of the three studied lakes. The 0.087 value comes from a large earthflow complex that borders the western and southern edge of the lake. When MADstd is calculated using a moving window of 5m, variations in MADstd across the earthflow complex become clear (Figure 5 inset). In particular, a higher MADstd region can be identified at the base of the lake, where a sharper headscarp and an offset logging road indicate reactivation of this part of the earthflow complex. The MADstd of the reactivated portion is 0.137, much higher than the 0.087 value for the earthflow complex as a whole. When the new value is used, we see that the three lakes cluster in a range of MADstd values of 0.137 to 0.146 with an age of approximately 250-500 years. Therefore, we conclude that earthflows active in the last few hundred years may have a range of MADstd of 0.137 to 0.146. When relatively dating earthflow activity, we should use MADstd differences of >0.01 to differentiate separate periods of earthflow activity.

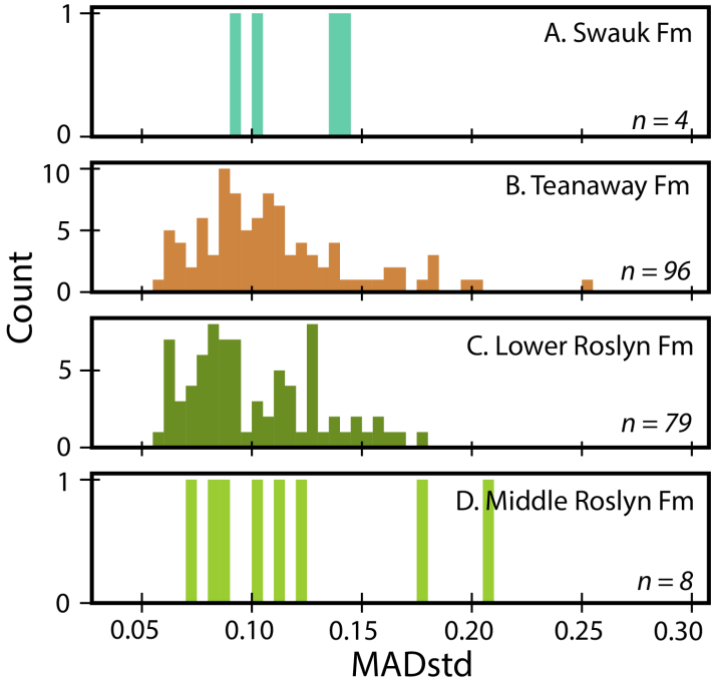

Figure 8. Distribution of MADstd values by lithology, binned by 0.05.

4.5 Relative earthflow activity

We analyze relative earthflow age by underlying lithology. Soil diffusion is the primarily control on the relationship between MADstd and earthflow activity (Figure 6); diffusion is set by climate (Sweeney et al., 2015) and lithology (Johnstone and

Hilley, 2015) which determine the rate of soil movement as well as soil thickness. The study area experiences similar climate, and so we can compare earthflows within each lithologic unit to contrast relative earthflow activity. Only five and eight earthflows are sourced in the Swauk or Middle Roslyn formations, respectively, and MADstd values range from 0.07 to 0.21 (Figure 6). The majority of earthflows (n=96) are underlain by the volcanic Teanaway Formation. MADstd values are clustered around 0.10, with a small frequency peak near 0.17. Unlike the mostly unimodal distribution in the Teanway Formation, earthflows in the lower Roslyn Formation have a bimodal MADstd distribution with peaks at 0.08 and 0.13.

Absolute ages suggest that earthflows active in the last few hundred years have MADstd values of 0.13 to 0.15, approximately (Figure 5), and that differences of >0.01 MADstd are necessary to distinguish between relative earthflow ages. Based on this, the earthflows underlain by the Teanaway Formation are mostly inactive but do contain some earthflows that have been active in the last few hundred years; 24 (25%) earthflows have MADstd of >0.13. For earthflows underlain by the Roslyn Formation, a similar percentage were likely active in the last few hundred years, with 20 (25%) earthflows with a MADstd of >0.13.

That the MADstd values for the lower Roslyn Formation are bimodal indicates the prevalence of active earthflows with MADstd of >0.13 is unlikely to be due to a preservation bias, nor to constant earthflow activity. Instead, the sharp break between active earthflows and the cluster of older earthflows around 0.08 MADstd suggests a history of: initial earthflow activity, followed by a cessation in which soil diffusion acted across earthflows, then re-activation or new earthflow formation of 25% of the earthflows in the study area.

5 Discussion

5.1 Drivers of earthflow motion

Our aspect analysis showed a strong preference for earthflows to be oriented towards the southwest quadrangle (Figure 3), and we hypothesize that this reflects a bedding plane control on earthflow location. The Roslyn and Teanaway Formations are gently dipping to the southwest with dip angles ranging from 10 to 30 degrees (Tabor et al., 1982), comparable to the modal and median earthflow slopes. There is some variability in the bedding orientation as the Teanaway and Roslyn formations curve to the west, but only 8.5 percent of earthflows by area are located in this southeast-dipping region. Southeast aspects account for 21% of mapped earthflows; this mismatch implies not all earthflows are directly aligned to underlying bedding planes. Possibly, southerly aspects could be preferential due to vegetation and evaporation conditions that affects hillslope stabilization. However, the hillslopes in our study area are uniformly *Pinus ponderosa* dominated forest. The preponderance of SW facing earthflows thus indicates that most earthflows are lithologically controlled. Since the Roslyn and Teanaway are conformable, the bedding plane orientation also reflects the mid-Eocene landscape surface, and therefore the orientation of paleosols within the two units. Previous work has noted that paleosols and volcanic flows interspersed in the Teanaway and Roslyn formations form planes of weakness for landslides (NFTWA, 1996). That our observed slopes and aspects match the

bedding orientation supports this finding and indicates the bedding provides a first-hand control on the orientation of earthflows in the Teanaway basin.

Further support for a lithologic control is the prevalence of earthflows in the Teanaway and lower Roslyn Formations, with 94% of mapped earthflows in these two units that make up 32.7% of the study area. The southern edge of mapped earthflows does align with the extent of Pleistocene glaciations, which overtopped the western drainage boundary and flowed in through the West Fork Teanaway. Although earthflows likely postdate the 120ky glaciation, the muted topography resulting from glacial erosion may be less prone to earthflows. The glacial extent overlaps both the middle and lower Roslyn Formation (Figure 2), and earthflows in the lower Roslyn Formation stop at the low relief topography left by glacial erosion. Thus, glacial erosion, in addition to underlying lithology, appears to control the extent of glaciation. At the southern edges of the study area, glacial erosion is minimal and topographic relief increases. However, only eight small earthflows were mapped in this region, which is underlain by middle and upper Roslyn Formation. Although conformable, the middle and upper Roslyn Formation members lack rhyolite interbeds and are finer grained in comparison to the lower member (Tabor et al., 1984). Likely, the interbedded rhyolite allows planes of weakness to form (NFTWA, 1996) that promote earthflow formation.

Our absolute and relative ages indicate approximately 25% (n = 46) of the mapped earthflows were active within the last few hundred years; however, we do not have strong age control for the remaining 141 earthflows. Earthflow activity is often correlated to climate, with wetter periods driving earthflow motion (Baum et al., 2003) and drier periods creating desiccation cracks that prime the landscape for deep water infiltration (McSaveney and Griffiths, 1987). The last few hundred years in the Teanaway basin were climatically characterized by the Little Ice Age, which caused about 1°C cooler conditions (Graumlich and Brubaker, 1986). This temperature change is unlikely to significantly alter weathering rates and regolith production (Marshall et al., 2015; Schanz et al., 2019), and precipitation rates remained low. However, human modification since 1890 may have contributed to earthflow activity. Starting c 1890, large scale deforestation and road building began (Kittitas County Centennial Committee, 1989), which would decrease evapotranspiration and root strength, leading to greater water infiltration and weaker soil cohesion; conditions that promote earthflow movement. Similar patterns are seen in the Waipaoa River basin, New Zealand, where deforestation in the last two hundred years has resulted in mass movements and increased sediment loads (Cerovski-Darriau and Roering, 2016).

5.2 Landscape disturbance

Earthflows in the Teanaway basin alter valley bottom topography and hillslope erosion rates, which affects habitat zones and Holocene denudation rates. In the Teanaway forks and mainstem, no earthflows encroach on the valley bottoms, but all of the North Fork tributaries examined in Figure 4 initiate on an earthflow or earthflow complex, with the exception of Jack and Dickey creeks. Only a relatively small number (10 of 187) of mapped earthflows in the North Fork tributaries are in direct

contact with streams; these earthflows range in size from a large earthflow complex of 4 km^2 to smaller flows of 14,000 m^2 and show mostly recent (<200 years) activity.

Increased sediment flux from earthflows appears to be mostly fine sediment; grain size surveys indicate high amounts of fine sediment and moderate coarse sediment loads in the North Fork tributaries with no significant difference between tributaries draining Teanaway and lower Roslyn formations, despite a rock strength difference between the basalt and friable sandstone (NFTWA, 1996). In a similar sandstone formation, Fratkin et al. (2020) found significant variation in surface and subsurface grain size when compared to adjacent tributaries draining basalt; most bedload in their study area was delivered by debris flows and landslides. However, earthflows tend to incorporate highly weathered material and regolith; in the Eel River, 90% of earthflow colluvium is smaller than 76 mm (Mackey and Roering, 2011). Field observations in the Teanaway at earthflow toes and exposed surfaces were of sand and silt size fractions, with a few small gravels, even at radiocarbon site 8-4-20-2, which had insufficient carbon to produce an age but is from an earthflow sourced entirely from the Teanaway Formation basalt. Thus, the abundant fine sediment and lack of significant grain size difference between tributaries in the Teanaway and lower Roslyn formation may reflect large sediment contributions from earthflows, which preferentially transport weathered regolith..

These effects on sediment flux and valley width are likely to disturb in-stream habitat. Heighted fine sediment delivery can clog pore spaces in spawning gravels; however, slopes in the Teanaway basin are high and sufficient to quickly transport sands and finer material downstream (NFTWA, 1996; Schanz et al., 2019). Floodplain habitat is reduced where earthflows narrow the valley (Figure 4), though valley widths are abnormally large just upstream of earthflows in Jungle, Rye and Dickey creeks. Valley width is a key landscape characteristic for salmon habitat (Burnett et al., 2007) and wider valleys are often associated with heterogeneous channel features (Montgomery and Buffington, 1997) and flood refuge habitat (May et al., 2013). That Teanaway earthflows can create heterogeneity in valley widths implies they exert a direct influence on riparian habitat.

5.3 MADstd as relative dating tool

Our lake sedimentation ages showed very little relationship between MADstd and earthflow activity for recent earthflows; however, this finding is consistent with other studies of landslide surface roughness. Comparing three surface roughness metrics on landslides spanning ~200 years of activity, Goetz et al. (2014) found no relationship between surface roughness and age. Booth et al. (2017) suggest surface roughness is more appropriately used to distinguish landslide ages at the scale of thousands of years. Thus, the limitations of MADstd are similar to other surface roughness metrics in that we cannot distinguish relative earthflow activity of <200 years.

Yet, MADstd is able to identify flow features and differentiate between forest terrain, which gives it an advantage over some other roughness metrics. The original flow directional MAD metric picks up flow features such as scarps, debris flows, and channels that are missed by isotropic roughness metrics (Trevisani and Cavalli, 2016). In the case of earthflows, high and low

flow directional MAD values are associated with the strong lineations; as flow follows the crests and hollows, the >1 m lineations also direct flow orthogonal to crests (Figure 6 inset). By taking the standard deviation, we can highlight the parallel and orthogonal flow that is characteristic of >1 m scale lineations; however, it is important to note that this method would not work if the elevation model resolution is greater than the lineation scale. Compared to other metrics applied to landslides, the MADstd includes a flow directional roughness and detrends the data, both of which have been found to improve landslide identification accuracy (Berti et al., 2013; McKean and Roering, 2004). Previously used surface roughness metrics often have trouble capturing the top of earthflows and differentiating between rough, forested terrain and landslide roughness (Berti et al., 2013). When the MADstd is calculated over a moving 5 m radius window, rather than over a single earthflow, forested hillslopes are clearly delineated from earthflows. The roughness elements from trees are isotropic and give MADstd values near zero (Figure 5 inset). The scarp, flowlines, and toe produce strong lineations in the landscape that light up in the MADstd plots, due to the parallel and orthogonal flow over the 1 m DEM. Even smaller earthflows, of approximately 3600 m^2, are identified with the 5 m moving window MADstd. This advantage over previous, isotropic methods of calculating surface roughness and identifying landslides indicates MADstd is an appropriate method for use in identifying and mapping earthflows, though we caution that the DEM resolution size must be less than the scale of earthflow lineations.

Further, the decay of MADstd with age shows potential, particularly if it can be used as an absolute age when combined with other dating methods. As time since earthflow activity increases, MADstd decreases in a strongly correlated (r-squared > 0.98) linear relationship. Any error in the linear relationship remains similar despite the time frame considered. In contrast, other surface roughness metrics like standard deviation of slope (SDS) have an exponential relationship with landslide age. When calibrated to absolute dating, exponential relationships can result in errors are up to ±1 ky for landslides that are 10 ky old (LaHusen et al., 2016). Although we were unable to convert the MADstd relationship to an absolute age relationship for the Teanaway, the MADstd roughness metric has potential as a more precise method to date older mass movements (~10 ky or greater).

6 Conclusion

To examine controls on earthflow activity and resulting topographic disturbance in the Teanaway basin, we mapped and dated earthflows using 1 m lidar and a new relative dating method that relies on flow directional surface roughness. The MADstd metric appears well-suited to identifying and relatively dating earthflows, as it picks up linear roughness elements such as lateral shear zones and levees, and is able to ignore the influence of dense vegetation on the elevation model. This is particularly useful for densely vegetated areas, where other roughness metrics have difficulty and where object tracking is problematic to apply. In addition to MADstd relative ages, we used radiocarbon and sedimentation ages to provide a few constraining absolute ages; these ages indicate that 25% of earthflows in the Teanaway basin were active in the last few hundred years. Nearly all (94%) of earthflows occur in the Teanaway and lower Roslyn formations, which contain interbedded basalt and rhyolite flows

along with paleosols and coarse sandstone. Slide aspect and slope roughly follow the orientation of the paleosol and volcanic flow dip angles, suggesting a strong lithologic control on earthflow location and orientation. Most tributaries in the Teanaway initiate on earthflow complexes, and experience valley width changes due to earthflow damming and associated upstream widening. Despite some variability in source lithology, the selective transport of regolith and weathered material by earthflows results in delivery of fine sediments. While this fine sediment poses a potential hazard for instream habitat, stream power is sufficient to transport it downstream; therefore, the largest habitat disturbance provided by the earthflows is heterogeneity in valley width.

Data and code availability

The diffusion simulation code and input files can be access on https://github.com/schanzs/JungleCk_diffusion. Landslide information and dates are available at: https://doi.org/10.5281/zenodo.5885660

Author contribution

SAS conceptualized the study, SAS and APC contributed equally to study design and methodology. APC and SAS acquired funding for the study. SAS wrote the paper with contributions from APC.

Competing interests

The authors declare that they have no conflict of interest.

Acknowledgements

Funding to APC was provided by the Patricia J. Buster grant from the Colorado College Geology Department and radiocarbon sample analysis was paid for by Colorado College. We thank Matt Cooney for GIS help, and Jamie and Catharine Colee for help in the field. Field work was conducted on the traditional territory of the Yakama and Wenatchi People.

References

Agee, J. K.: Fire and weather disturbances in terrestrial ecosystems of the eastern Cascades, US. Department of Agriculture, Pacific Northwest Research Station, 1994.

Agee, J. K.: Fire Ecology of Pacific Northwest Forests, Island Press, 513 pp., 1996.

Baum, R., Savage, W., and Wasowski, J.: Mechanics of earth flows, Proc. Int. Conf. FLOWS Sorrento Italy, 2003.

Beeson, H. W., Flitcroft, R. L., Fonstad, M. A., and Roering, J. J.: Deep-Seated Landslides Drive Variability in Valley Width and Increase Connectivity of Salmon Habitat in the Oregon Coast Range, JAWRA J. Am. Water Resour. Assoc., 54, 1325–1340, https://doi.org/10.1111/1752-1688.12693, 2018.

Berti, M., Corsini, A., and Daehne, A.: Comparative analysis of surface roughness algorithms for the identification of active landslides, Geomorphology, 182, 1–18, https://doi.org/10.1016/j.geomorph.2012.10.022, 2013.

Booth, A. M., LaHusen, S. R., Duvall, A. R., and Montgomery, D. R.: Holocene history of deep-seated landsliding in the North Fork Stillaguamish River valley from surface roughness analysis, radiocarbon dating, and numerical landscape evolution modeling, 122, 456–472, https://doi.org/10.1002/2016JF003934, 2017.

Braun, J. and Willett, S. D.: A very efficient O(n), implicit and parallel method to solve the stream power equation governing fluvial incision and landscape evolution, Geomorphology, 180–181, 170–179, https://doi.org/10.1016/j.geomorph.2012.10.008, 2013.

Burnett, K. M., Reeves, G. H., Miller, D. J., Clarke, S., Vance-Borland, K., and Christiansen, K.: Distribution of Salmon-Habitat Potential Relative to Landscape Characteristics and Implications for Conservation, Ecol. Appl., 17, 66–80, https://doi.org/10.1890/1051-0761(2007)017[0066:DOSPRT]2.0.CO;2, 2007.

Cerovski-Darriau, C. and Roering, J. J.: Influence of anthropogenic land-use change on hillslope erosion in the Waipaoa River Basin, New Zealand, 41, 2167–2176, https://doi.org/10.1002/esp.3969, 2016.

Cle Elum Tribune: Cle Elum Tribune, March 20, 1891 issue, , 20th March, page 4, 1891.

Coe, J. A.: Regional moisture balance control of landslide motion: Implications for landslide forecasting in a changing climate, Geology, 40, 323–326, https://doi.org/10.1130/G32897.1, 2012.

Fratkin, M. M., Segura, C., and Bywater-Reyes, S.: The influence of lithology on channel geometry and bed sediment organization in mountainous hillslope-coupled streams, 45, 2365–2379, https://doi.org/10.1002/esp.4885, 2020.

Goetz, J. N., Bell, R., and Brenning, A.: Could surface roughness be a poor proxy for landslide age? Results from the Swabian Alb, Germany, 39, 1697–1704, https://doi.org/10.1002/esp.3630, 2014.

Graumlich, L. J. and Brubaker, L. B.: Reconstruction of annual temperature (1590–1979) for Longmire, Washington, derived from tree rings, 25, 223–234, 1986.

Guerriero, L., Bertello, L., Cardozo, N., Berti, M., Grelle, G., and Revellino, P.: Unsteady sediment discharge in earth flows: A case study from the Mount Pizzuto earth flow, southern Italy, Geomorphology, 295, 260–284, https://doi.org/10.1016/j.geomorph.2017.07.011, 2017.

Handwerger, A. L., Roering, J. J., and Schmidt, D. A.: Controls on the seasonal deformation of slow-moving landslides, Earth Planet. Sci. Lett., 377–378, 239–247, https://doi.org/10.1016/j.epsl.2013.06.047, 2013.

Hungr, O., Leroueil, S., and Picarelli, L.: The Varnes classification of landslide types, an update, Landslides, 11, 167–194, https://doi.org/10.1007/s10346-013-0436-y, 2014.

Johnstone, S. A. and Hilley, G. E.: Lithologic control on the form of soil-mantled hillslopes, Geology, 43, 83–86, https://doi.org/10.1130/G36052.1, 2015.

Kittitas County Centennial Committee: A history of Kittitas County, Washington, Taylor Publishing Company, Dallas, TX, 693 pp., 1989.

LaHusen, S. R., Duvall, A. R., Booth, A. M., and Montgomery, D. R.: Surface roughness dating of long-runout landslides near Oso, Washington (USA), reveals persistent postglacial hillslope instability, Geology, 44, 111–114, https://doi.org/10.1130/G37267.1, 2016.

Mackey, B. H. and Roering, J. J.: Sediment yield, spatial characteristics, and the long-term evolution of active earthflows determined from airborne LiDAR and historical aerial photographs, Eel River, California, GSA Bull., 123, 1560–1576, https://doi.org/10.1130/B30306.1, 2011.

Malet, J.-P., Laigle, D., Remaître, A., and Maquaire, O.: Triggering conditions and mobility of debris flows associated to complex earthflows, Geomorphology, 66, 215–235, https://doi.org/10.1016/j.geomorph.2004.09.014, 2005.

Marshall, J. A., Roering, J. J., Bartlein, P. J., Gavin, D. G., Granger, D. E., Rempel, A. W., Praskievicz, S. J., and Hales, T. C.: Frost for the trees: Did climate increase erosion in unglaciated landscapes during the late Pleistocene?, Sci. Adv., 1, e1500715, https://doi.org/10.1126/sciadv.1500715, 2015.

Martin, Y.: Modelling hillslope evolution: linear and nonlinear transport relations, Geomorphology, 34, 1–21, https://doi.org/10.1016/S0169-555X(99)00127-0, 2000.

May, C., Roering, J., Eaton, L. S., and Burnett, K. M.: Controls on valley width in mountainous landscapes: The role of landsliding and implications for salmonid habitat, Geology, 41, 503–506, https://doi.org/10.1130/G33979.1, 2013.

McKean, J. and Roering, J.: Objective landslide detection and surface morphology mapping using high-resolution airborne laser altimetry, Geomorphology, 57, 331–351, https://doi.org/10.1016/S0169-555X(03)00164-8, 2004.

McSaveney, M. J. and Griffiths, G. A.: Drought, rain, and movement of a recurrent earthflow complex in New Zealand, Geology, 15, 643–646, https://doi.org/10.1130/0091-7613(1987)15<643:DRAMOA>2.0.CO;2, 1987.

Montgomery, D. R. and Buffington, J. M.: Channel-reach morphology in mountain drainage basins, Geol. Soc. Am. Bull., 109, 596–611, 1997.

Moon, S., Page Chamberlain, C., Blisniuk, K., Levine, N., Rood, D. H., and Hilley, G. E.: Climatic control of denudation in the deglaciated landscape of the Washington Cascades, Nat. Geosci., 4, 469–473, https://doi.org/10.1038/ngeo1159, 2011.

Nereson, A. L. and Finnegan, N. J.: Drivers of earthflow motion revealed by an 80 yr record of displacement from Oak Ridge earthflow, Diablo Range, California, USA, GSA Bull., 131, 389–402, https://doi.org/10.1130/B32020.1, 2018.

NFTWA: North Fork Teanaway Watershed Analysis: Resource Assessment Report. Prepared by: Boise Cascade Corporation; Cascade Environmental Services, Inc.; Mary Raines, Geomorphologist; Shannon & Wilson, Inc.; Karen F. Welch, Hydrologist; Forster Wheeler; Caldwell & Associates; Ecologic, Inc.; Yakama Indian Nation; EDAW, Inc., Boise, ID., 1996.

Porter, S. C.: Pleistocene glaciation in the southern part of the North Cascade Range, Washington, Geol. Soc. Am. Bull., 87, 61–75, https://doi.org/10.1130/0016-7606(1976)87<61:PGITSP>2.0.CO;2, 1976.

Quantum Spatial: Teanaway streams topobathymetric LiDAR, 2015.

Quantum Spatial: Yakima Wildfire Lidar Survey, Available at: https://lidarportal.dnr.wa.gov/. Accessed on May 24, 2021, 2018.

Reimer, P. J., Austin, W. E. N., Bard, E., Bayliss, A., Blackwell, P. G., Ramsey, C. B., Butzin, M., Cheng, H., Edwards, R. L., Friedrich, M., Grootes, P. M., Guilderson, T. P., Hajdas, I., Heaton, T. J., Hogg, A. G., Hughen, K. A., Kromer, B., Manning, S. W., Muscheler, R., Palmer, J. G., Pearson, C., Plicht, J. van der, Reimer, R. W., Richards, D. A., Scott, E. M., Southon, J. R., Turney, C. S. M., Wacker, L., Adolphi, F., Büntgen, U., Capano, M., Fahrni, S. M., Fogtmann-Schulz, A., Friedrich, R., Köhler, P., Kudsk, S., Miyake, F., Olsen, J., Reinig, F., Sakamoto, M., Sookdeo, A., and Talamo, S.: The IntCal20 Northern Hemisphere Radiocarbon Age Calibration Curve (0–55 cal kBP), Radiocarbon, 62, 725–757, https://doi.org/10.1017/RDC.2020.41, 2020.

Reiners, P. W., Ehlers, T. A., Mitchell, S. G., and Montgomery, D. R.: Coupled spatial variations in precipitation and long-term erosion rates across the Washington Cascades, Nature, 426, 645–647, https://doi.org/10.1038/nature02111, 2003.

Schanz, S. A., Montgomery, D. R., and Collins, B. D.: Anthropogenic strath terrace formation caused by reduced sediment retention, Proc. Natl. Acad. Sci., 116, 8734–8739, https://doi.org/10.1073/pnas.1814627116, 2019.

Struble, W. T., Roering, J. J., Black, B. A., Burns, W. J., Calhoun, N., and Wetherell, L.: Dendrochronological dating of landslides in western Oregon: Searching for signals of the Cascadia A.D. 1700 earthquake, GSA Bull., 132, 1775–1791, https://doi.org/10.1130/B35269.1, 2020.

Sweeney, K. E., Roering, J. J., and Ellis, C.: Experimental evidence for hillslope control of landscape scale, https://doi.org/10.1126/science.aab0017, 2015.

Tabor, R. W., Waitt, Jr., R. B., Frizzell, Jr., V. A., Swanson, D. A., Byerly, G. R., and Bentley, R. D.: Geologic map of the Wenatchee 1:100,000 quadrangle, central Washington, U.S. Geological Survey, Menlo Park, CA, 1982.

Tabor, R. W., Frizzel, V. A., JR., Vance, J. A., and Naeser, C. W.: Ages and stratigraphy of lower and middle Tertiary sedimentary and volcanic rocks of the central Cascades, Washington: Application to the tectonic history of the Straight Creek fault, GSA Bull., 95, 26–44, https://doi.org/10.1130/0016-7606(1984)95<26:AASOLA>2.0.CO;2, 1984.

Trevisani, S. and Cavalli, M.: Topography-based flow-directional roughness: potential and challenges, Earth Surf. Dyn., 4, 343–358, https://doi.org/10.5194/esurf-4-343-2016, 2016.

Trevisani, S. and Rocca, M.: MAD: robust image texture analysis for applications in high resolution geomorphometry, Comput. Geosci., 81, 78–92, https://doi.org/10.1016/j.cageo.2015.04.003, 2015.

U.S. Geological Survey: The StreamStats program for Washington: http://water.usgs.gov/osw/streamstats/Washington.html, last access: 5 January 2018, 2012.

Waples, R. S., Pess, G. R., and Beechie, T.: Evolutionary history of Pacific salmon in dynamic environments, Evol. Appl., 1, 189–206, https://doi.org/10.1111/j.1752-4571.2008.00023.x, 2008.

Wright, C. S. and Agee, J. K.: Fire and Vegetation History in the Eastern Cascade Mountains, Washington, Ecol. Appl., 14, 443–459, https://doi.org/10.1890/02-5349, 2004.